Journal of the Brazilian Society of Mechanical Sciences and Engineering (2018) 40:379
https://doi.org/10.1007/s40430-018-1296-0

TECHNICAL PAPER

Surface characterization of zirconia ceramics in ultrasonic vibration-assisted grinding

Zhihua Li[1] · Kan Zheng[1] · Wenhe Liao[1] · Xingzhi Xiao[1]

Received: 6 February 2018 / Accepted: 6 July 2018 / Published online: 14 July 2018

Abstract
In order to clarify the surface features of zirconia ceramics fabricated by ultrasonic vibration-assisted grinding (UVAG), five geometric parameters (width d_w, depth h_d, length l_d, spacing d_f and number N) of UVAG surface are selected to characterize UVAG surface topography. In this study, firstly, the mathematic modeling between five geometric parameters and grinding parameters (spindle speed, feed rate, cutting depth and power ratio) is revealed considering the overlapping of entire grains on the end face of tool. The expected value of center-to-center distance between two successive grooves, k_0, k_1, k_2, k_3 and k_4 are introduced to consider the effect of overlapping. Besides, the experiments of UVAG on zirconia ceramics are carried out to verify the theoretical values of width d_w, depth h_d, length l_d, spacing d_f and number N. Finally, it is found that the theoretical values and experimental values are well consistent with each other. Therefore, this mathematic modeling can be applied to characterize surface topography in UVAG of zirconia ceramics.

Keywords Surface characterization · Zirconia ceramics · Surface topography · Ultrasonic vibration-assisted grinding · Overlapping of grains

1 Introduction

Zirconia ceramics has obvious advantages in dental prosthodontics with the consideration of their excellent mechanical strength, outstanding wear resistance, superior esthetics, and so on [1–3]. However, when zirconia ceramics as a denture chews in the oral cavity, friction and wear is unavoidable [4, 5]. Liu et al. [6] investigated the friction and wear phenomenon between zirconia and natural enamel, and fatigue wear was found. Wang et al. conducted tribological tests of dental ceramics, and the results showed that the abrasive wear appeared [7]. There are two ways to reduce friction and wear which are the improvement in surface topography and lubricant. But the improvement in saliva in the oral cavity is difficult to put into practice. Thus, surface topography enhancement of zirconia ceramics is applied to the field of dental prosthodontics. Many investigations have indicated that surface topography feature is the key factor that affects friction and wear performance [8–10]. Li et al. [11] fabricated microdimple on copper surface by laser peen texturing (LPT), and it showed that friction coefficient with surface texture density of 13% could be decreased up to about 50% compared with that of untextured surface. Tang et al. [12] experimentally researched the relationship between surface texturing and friction and wear performance, and it had been known that friction could be reduced by 38%, while wear was decreased up to 72% when the dimple area fraction was 5%. Segu et al. [13] had created patterned microstructures by laser surface texturing technology, it presented friction coefficient with textured surface was lower than that with untextured surface, and dimple depth had an effect on friction coefficients reduction. From the above researches, it can be seen that there is a close link between surface topography and friction and wear performance. Therefore, it is necessary to fabricate suitable surface to improve friction and wear phenomenon.

Ultrasonic vibration-assisted grinding (UVAG) technology has been verified that it has outstanding advantages

Technical Editor: Márcio Bacci da Silva.

✉ Kan Zheng
zhengkan@njust.edu.cn

[1] School of Mechanical Engineering, Nanjing University of Science and Technology, Nanjing City 210094, Jiangsu Province, China

(long cutting life, low cutting force and so on) to fabricate hard and brittle materials [14–18]. For these advantages, in dental prosthodontics, UVAG technology is applied to fabricate ceramics restorations [19]. UVAG surface topography shows uniform and discontinuous grooves which have relationship with friction and wear performance [19]. Thus, in order to control friction and wear phenomenon of zirconia ceramics in dental prosthodontics, it is necessary to clarify the UVAG surface features. A series of researches have been conducted to clarify the UVAG surface quality and surface feature. Yan et al. [20] conducted two-dimensional ultrasonic-assisted grinding and diamond grinding experiments, surface roughness Ra was used to characterize surface quality, and it was 0.081 μm after UVAG, while it was 0.162 μm after DG. Guo et al. [21] introduced ultrasonic vibration-assisted grinding (UVAG) to machining microstructured surfaces and explained the relationship between cutting paraments and microstructured surface, the results showed that ultrasonic vibration could keep the edge sharpness of the microstructure, and there was no significant impact on microstructured surface roughness when spindle speed was from 1000 to 3000 rpm. However, quantitative relationships between geometric parameters on UVAG surface and grinding parameters have not been attained in these researches. While the quantitative relationships can be employed to design the surface topography in UVAG considering industrial demand, they provide a deep understanding of UVAG processing. Therefore, combined with friction and wear properties, five geometric parameters are proposed for UVAG surface in this paper. First of all, five geometric parameters are chosen to describe UVAG surface topography. The quantitative relationships between five geometric parameters and grinding parameters are proposed. Besides, UVAG verification tests are conducted on zirconia ceramics.

This study is made up of four sections. This section is introduction section. The quantitative relationships between five geometric parameters and grinding parameters are given in Sect. 2. UVAG verification tests are carried out to validate the quantitative relationships in Sect. 3. Conclusions are given in Sect. 4.

2 Surface topography model during UVAG

It has been proved that there are uniform and discontinuous grooves on the surface machined by UVAG [19]. In order to clearly illustrate these surface features, five geometric parameters are selected, which are width, depth, length of a single groove, spacing between two adjacent grooves in the feed direction on the UVAG surface and the number of grooves with the measured scale of 100 μm × 100 μm. The list of symbols in this work is given in Table 1.

2.1 Zirconia ceramics removal mechanism of a single grain during UVAG

UVAG technology is the complex cutting process of the entire grains on the end of the tool, as shown in Fig. 1. Kinematics analysis of a single grain is selected to clarify kinematic relationships in UVAG. It is expressed as:

$$\begin{cases} S_x = V_s t + r\cos(\omega t) \\ S_y = r\sin(\omega t) \\ S_z = A\sin(2\pi f t) \end{cases} \tag{1}$$

where f means ultrasonic vibration frequency, Hz; A is ultrasonic amplitude, μm; r denotes the rotational radius of a grain, mm; ω is angular velocity of a grain, rad/s; feed rate is V_s, mm/s; t is the cutting time of a grain, s.

According to the crack system of a single grain of zirconia ceramics, it can be known that the width C_{L0} and depth C_{h0} of the lateral crack can be presented by the following equation [22]:

$$C_{L0} = C_2\left(\tan\frac{\beta}{2}\right)^{\frac{-5}{12}}\cdot\left[\frac{E^{\frac{3}{4}}}{H_v K_{IC}(1-\upsilon^2)^{\frac{1}{2}}}\right]^{\frac{1}{2}}\cdot F^{\frac{5}{8}} \tag{2}$$

$$C_{h0} = C_2\left(\tan\frac{\beta}{2}\right)^{-\frac{1}{3}}\cdot\frac{E^{\frac{1}{2}}}{H_v}\cdot F^{\frac{1}{2}} \tag{3}$$

where F is the force of a single grain, N; $C_2 = 0.226$ [22]; υ denotes Poisson's ratio of zirconia ceramics with β which is the apex angel of a single grain; K_{IC} means fracture strength of zirconia ceramics, $MPam^{1/2}$; E is the Young's modulus, MPa; H_v is the hardness, MPa.

The total force of entire grains can be obtained as [23]:

$$F_N = C_0^{\frac{1}{8}}\cdot C_2^{\frac{-15}{8}}\cdot e^{\frac{-1}{8}}\cdot C_a^{\frac{1}{12}}\cdot K_0\cdot K_1^{\frac{7}{8}}\cdot\frac{(R_2^2-R_1^2)^{\frac{1}{8}}}{(R_2+R_1)^{\frac{7}{8}}}\cdot\left(\frac{D_2\cdot V_s}{n}\right)^{\frac{7}{8}} \cdot\frac{(A+a_p)^{\frac{7}{8}}}{A^{\frac{1}{8}}}\cdot\frac{H_v^{\frac{21}{16}}\cdot K_{IC}^{\frac{1}{2}}\cdot(1-\upsilon^2)^{\frac{1}{4}}}{E^{\frac{13}{16}}\cdot\left(\tan\frac{\beta}{2}\right)^{\frac{13}{16}}} \tag{4}$$

where n is spindle speed, r/min; a_p means cutting depth, mm; $K_0 = 2^{-33/16}\times 360^{7/8}\times\xi^{1/16}\times\pi^{-7/8} = 14.60$; $K_1 = 0.064n^{0.5738}\cdot V_s^{-0.8564}\cdot a_p^{-0.5313}$; $C_0 = [3\times 0.88\times 10^{-3}/(100\times 2^{0.5}\rho)]^{2/3}$; D_2 is the outer diameter of tool, mm; R_2 is the outer radius, mm; R_1 denotes the inner radius, mm; ρ means density of zirconia ceramics, g/cm^3; C_a is the concentration of grains; e means the grain size, mm.

The effective grain number is expressed as:

Table 1 List of symbols

Symbols	Meaning
f	Ultrasonic vibration frequency, Hz
A	Ultrasonic amplitude, μm
r	Rotational radius of the grain, mm
ω	Angular velocity of the grain, rad/s
V_s	Feed rate, mm/s
t	Cutting time of a gain, s
S_x	Cutting distance in x direction of a grain, mm
S_y	Cutting distance in y direction of a grain, mm
S_z	Cutting distance in z direction of a grain, mm
F	Force of a single grain, N
C_2	Dimensionless constant, 0.226
υ	Poisson's ratio of zirconia ceramics
β	Apex angel of a single grain, °
K_{IC}	Fracture strength of zirconia ceramics, MPa
E	Young's modulus of zirconia ceramics, MPa
H_v	Hardness of zirconia ceramics, MPa
C_{L0}	Width of the lateral crack, mm
C_{h0}	Depth of the lateral crack, mm
F_N	Total force of entire grains, N
n	Spindle speed, r/min
a_p	Cutting depth, mm
K_0	Dimensionless constant, 14.60
K_1	Dimensionless constant, related to cutting parameters
C_0	Dimensionless constant, related to ρ
D_2	Outer diameter of tool, mm
R_2	Outer radius of tool, mm
R_1	Inner radius of tool, mm
ρ	Density of zirconia ceramics, g/cm^3
C_a	Concentration of grains
e	Grain size, mm
N_{all}	Effective grain number
t_{valid}	Effective cutting time, s
δ	Maximum cutting depth of a grain, mm
ξ	1.85
l_0	Effective cutting length of one grain in a certain period, mm
$f(r)$	Probability density function
Δd	Distance of center line between two successive grooves fabricated by two adjacent grains, mm
$f(d_1,d_2)$	A joint probability density function
J	Jacobian determinant
$E(\Delta d)$	Expected value of Δd
d_{w1}	Width of the overlapping groove, mm
d_w	Actual width of one groove, mm
h_d	Actual depth of one groove, mm
l_d	Actual length of one groove, mm
k	Power ratio
k_0	Overlapping parameters related to cutting parameters
k_1	Overlapping parameters related to cutting parameters
k_2	Overlapping parameters related to cutting parameters
T	Rotating period of the tool, s
Δd_1	Spacing between two grooves fabricated by a single grain in unit period in the feed direction, mm
d_f	Spacing between two grooves on the surface, mm
T_0	Vibration period, s
N_1	Number of grooves in one rotating period
N	Number of in unit area (100 μm × 100 μm) on the surface
k_3	Overlapping parameters related to cutting parameters
k_4	Overlapping parameters related to cutting parameters

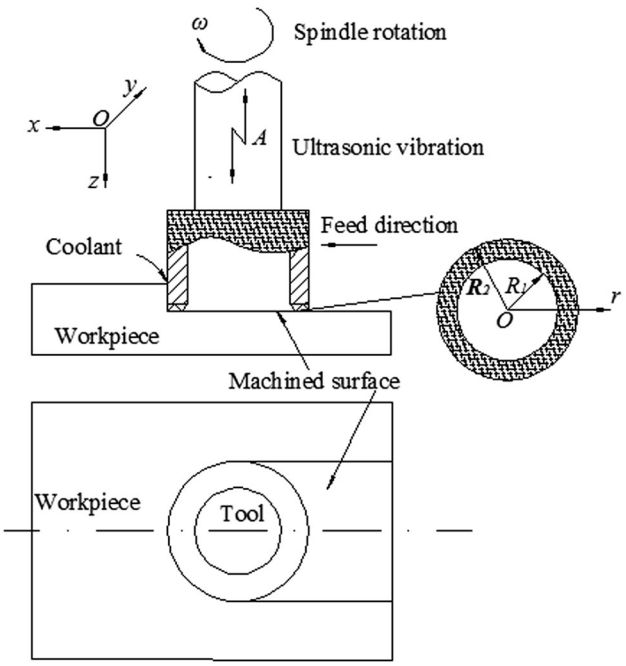

Fig. 1 Kinematic relationship in UVAG

$$N_{all} = C_0 \frac{C_a^{\frac{2}{3}}}{e^2} \pi R_2^2. \tag{5}$$

Thus, the force of a single grain can be derived as:

$$F = \frac{F_N}{N_{all}} = C_0^{\frac{-7}{8}} \cdot C_2^{\frac{-15}{8}} \cdot e^{\frac{15}{8}} \cdot C_a^{\frac{-7}{12}} \cdot R_2^{-2} \cdot K_0 \cdot \pi^{-1} \cdot K_1^{\frac{7}{8}} \cdot \frac{\left(R_2^2 - R_1^2\right)^{\frac{1}{8}}}{(R_2 + R_1)^{\frac{7}{8}}} \cdot \left(\frac{D_2 \cdot V_s}{n}\right)^{\frac{7}{8}} \cdot \frac{\left(A + a_p\right)^{\frac{7}{8}}}{A^{\frac{1}{8}}} \cdot \frac{H_v^{\frac{21}{16}} \cdot K_{IC}^{\frac{1}{2}} \cdot (1 - \upsilon^2)^{\frac{1}{4}}}{E^{\frac{13}{16}} \cdot \left(\tan\frac{\beta}{2}\right)^{\frac{13}{16}}}. \tag{6}$$

Substituting Eq. 6 into Eqs. 2 and 3, C_{L0} and C_{h0} can be calculated as:

$$C_{L0} = m \cdot n^{-0.2599} \cdot V_s^{0.07853} \cdot a_p^{-0.2906} \cdot \left(A + a_p\right)^{0.5469} \cdot A^{-0.07813} \tag{7}$$

where

$$m = 0.1087 \cdot C_2^{-0.1719} \cdot \left(\tan\frac{\beta}{2}\right)^{-0.5339} \cdot E^{-0.1328} \cdot H_v^{0.3203} \cdot K_{IC}^{-0.1875} \cdot \left(1 - \upsilon^2\right)^{-0.09375} \cdot K_0^{0.625} \cdot C_0^{-0.5469} \cdot C_a^{-0.3646} \cdot e^{1.1719} \cdot R_2^{-1.25} \cdot D_2^{0.5469} \cdot \left(R_2^2 - R_1^2\right)^{0.07813} \cdot (R_2 + R_1)^{-0.5469}$$

$$C_{h0} = m_1 \cdot n^{-0.1865} \cdot V_s^{-0.06207} \cdot a_p^{-0.2324} \cdot \left(A + a_p\right)^{0.4375} \cdot A^{-0.0625} \tag{8}$$

where

$$m_1 = 0.1664 \cdot C_2^{0.0625} \cdot \left(\tan\frac{\beta}{2}\right)^{-0.7396} \cdot E^{0.09375} \cdot H_v^{-0.3438} \cdot K_0^{0.5} \cdot C_0^{-0.4375} \cdot C_a^{-0.2917} \cdot e^{0.9375} \cdot R_2^{-1} \cdot D_2^{0.4375} \cdot \left(R_2^2 - R_1^2\right)^{0.0625} \cdot (R_2 + R_1)^{-0.4375}.$$

Since UVAG is an interrupted cutting process, the effective cutting time can be expressed as [23]:

$$t_{valid} = \frac{1}{\pi f} \cdot \left[\frac{\pi}{2} - \arcsin\left(1 - \frac{\delta}{A}\right)\right] \tag{9}$$

where δ is the maximum cutting depth of a grain.

δ can be derived as [23]:

$$\delta^2 = \frac{720K_1\left(A + a_p\right) \cdot D_2 \cdot V_s \cdot A \cdot e}{\left(\frac{1}{2}\xi\right)^{\frac{1}{2}} \cdot C_2 \cdot C_0 \cdot C_a^{\frac{2}{3}} \cdot \pi n \cdot (R_2 + R_1)^2 \cdot (R_2 - R_1)} \cdot \frac{H_v^{\frac{1}{2}}}{E^{\frac{1}{2}} \cdot \left(\tan\frac{\beta}{2}\right)^{\frac{1}{6}}} \tag{10}$$

where ξ = 1.85.

Therefore, the effective cutting length of one grain in a certain period can be derived as:

$$l_0 = \frac{2\pi nr}{60} \cdot t_{valid} \tag{11}$$

where r is the rotational radius of the grain, mm.

Substituting Eqs. (9) and (10) into Eq. (11), the effective cutting length l_o can be obtained as:

$$l_0 = \frac{2nr}{60} \cdot \frac{1}{f} \cdot \left[\frac{\pi}{2} - \arcsin\left(1 - \frac{720^{\frac{1}{2}}K_1^{\frac{1}{2}}\left(A + a_p\right)^{\frac{1}{2}}D_2^{\frac{1}{2}}V_s^{\frac{1}{2}}e^{\frac{1}{2}}}{\left(\frac{1}{2}\xi\right)^{\frac{1}{4}}C_2^{\frac{1}{2}}C_0^{\frac{1}{2}}C_a^{\frac{1}{3}}\pi^{\frac{1}{2}}n^{\frac{1}{2}}A^{\frac{1}{2}}(R_2 + R_1)(R_2 - R_1)^{\frac{1}{2}}} \cdot \frac{H_v^{\frac{1}{4}}}{E^{\frac{1}{4}}\left(\tan\frac{\beta}{2}\right)^{\frac{1}{12}}}\right)\right] \tag{12}$$

Thus, according to the above analysis, it can be known the size of a groove (the width $2C_{L0}$, the depth C_{h0} and the effective cutting length l_0) which is formed by the crack system and the movement of one grain in a period, as shown in Fig. 2. Actually, interference is inevitable under the actual conditions. Therefore, interference phenomenon is analyzed by the following sections:

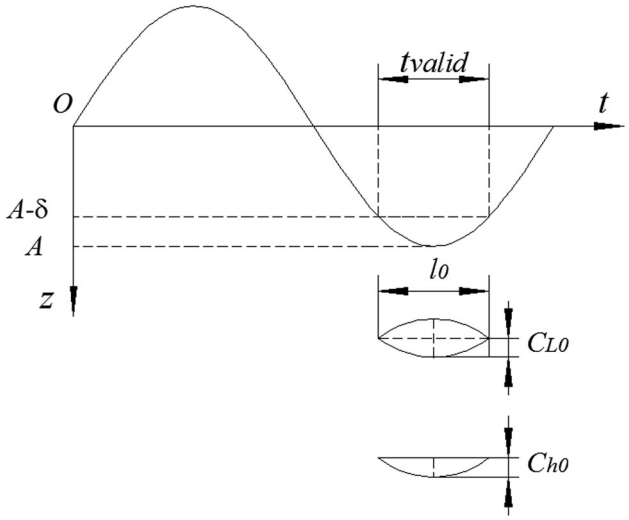

Fig. 2 Schematic illustration of a groove in one period

2.2 Analysis of actual width, depth and length of one groove on the surface based on overlapping

Assuming that the distribution of grains is uniform, the probability density function $f(r)$ can be obtained as:

$$f(r) = \frac{1}{R_2}. \tag{13}$$

The distance of centerline between two successive grooves fabricated by two adjacent grains can be expressed as:

$$\Delta d = |r_{x+1} - r_x| \tag{14}$$

where x means the xth groove.

Set $r_x = d_2$, $r_{x+1} = d_1 + d_2$, as shown in Fig. 3. d_1 and d_2 can be presented as:

$$d_1 = r_{x+1} - r_x \tag{15}$$

$$d_2 = r_x \tag{16}$$

From Eqs. (14) and (15), it can be known that $\Delta d = |d_1|$.

The probability density function of Δd can be expressed as:

$$P(|d_1| \le \Delta d) = P(d_1 \le -\Delta d) + P(d_1 \le -\Delta d). \tag{17}$$

The expected value of Δd can be calculated by a joint probability density function $f(d_1,d_2)$ which can be presented as:

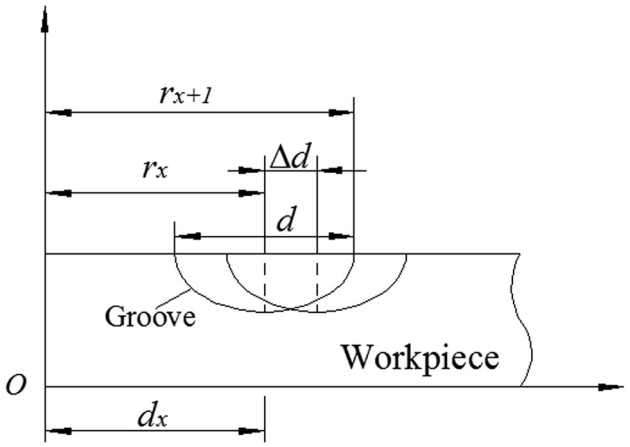

Fig. 3 Schematic illustration of two successive grooves

$$f(d_1, d_2) = f(r_1(d_1, d_2), r_2(d_1, d_2))|J| \tag{18}$$

where J denotes the Jacobian determinant.

Therefore, from the above analysis, the expected value of Δd can be calculated by the following equations:

$$E(\Delta d) = \int_0^d \Delta d \cdot f(\Delta d) d(\Delta d) = \frac{1}{3} d \tag{19}$$

where d is $2C_{L0}$.

$$E(\Delta d) = \frac{1}{3} d = \frac{1}{3} \cdot 2C_{L0} = \frac{2}{3} C_{L0} \tag{20}$$

According to Eq. (20), the two successive overlapping grooves are described in Fig. 4. The overlapping of grooves in radial direction is caused by random distribution of grains in radial direction. The width d_{w1} of the overlapping groove can be derived as:

$$d_{w1} = C_{L0} + \frac{2}{3} C_{L0} + C_{L0} = \frac{8}{3} C_{L0}. \tag{21}$$

During the actual UVAG process, the actual width d_w, depth h_d and length l_d of one groove on the surface are affected by the overlapping of different grains which depends on grinding parameters (spindle speed n, feed rate V_s, cutting depth a_p and power ratio k). It means that there are some differences between d_w, h_d, l_d and d_{w1}, C_{h0}, l_0. In order to solve this problem, overlapping parameters k_0 ($k_0 = c_0 n^{a_{10}} V_s^{a_{20}} a_p^{a_{30}} k^{a_{40}}$), k_1 ($k_1 = c_1 n^{a_{11}} V_s^{a_{21}} a_p^{a_{31}} k^{a_{41}}$) and k_2 ($k_2 = c_2 n^{a_{12}} V_s^{a_{22}} a_p^{a_{32}} k^{a_{42}}$) are introduced. Thus, the actual width d_w, depth h_d and length l_d can be expressed as:

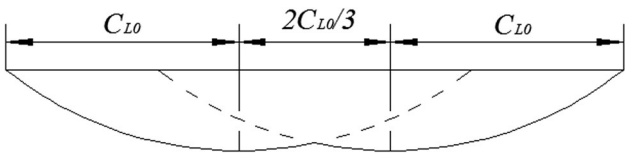

Fig. 4 Two successive overlapping grooves

$$d_w = k_0 \cdot d_{w1} \tag{22}$$

$$h_d = k_1 C_{h0} \tag{23}$$

$$l_d = k_2 \cdot l_0. \tag{24}$$

2.3 Analysis of spacing between two grooves on the surface

From Eq. (1), the kinematic equation of a single abrasive grain in the feed direction can be obtained as:

$$S(x) = V_s t + r \cos(2\pi n t). \tag{25}$$

When time is t_0, Eq. (25) can be derived as:

$$S(x_0) = V_s t_0 + r \cos(2\pi n t_0). \tag{26}$$

When time is $t_0 + T$, Eq. (25) can be derived as:

$$S(x_1) = V_s(t_0 + T) + r \cos(2\pi n(t_0 + T)) \tag{27}$$

where T is the rotating period of the tool, s,

$$T = \frac{1}{n}. \tag{28}$$

Thus, the spacing Δd_1 between two grooves fabricated by a single grain in unit period in the feed direction can be obtained as:

$$\Delta d_1 = S(x_1) - S(x_0) = \frac{V_s}{n}. \tag{29}$$

During the actual UVAG process, the spacing d_f between two grooves on the surface is affected by the overlapping of different grains which depends on grinding parameters (spindle speed n, feed rate V_s, cutting depth a_p and power ratio k). In order to solve this problem, an overlapping parameter k_3 ($k_3 = c_3 n^{a_{13}} V_s^{a_{23}} a_p^{a_{33}} k^{a_{43}}$) is introduced. Therefore, the spacing d_f between two grooves on the surface can be presented as:

$$d_f = k_3 \cdot \Delta d_1. \tag{30}$$

2.4 Analysis of number of grooves on the surface

During UVAG, there is an ultrasonic vibration. The vibration period T_0 can be expressed as:

$$T_0 = \frac{1}{f} \tag{31}$$

where f is ultrasonic vibration frequency, Hz.

Thus, the number N_1 of grooves in one rotating period can be obtained as:

$$N_1 = \frac{T}{T_0} = \frac{f}{n} \tag{32}$$

Table 2 Mechanical properties of zirconia ceramics

Property	Unit	Value
Bending strength	MPa	800–1000
Fracture toughness	MPa*m$^{1/2}$	6
Breaking strength	MPa	1200
Elastic modulus	GPa	210
Vickers hardness	GPa	12
Density	g/cm^3	6.05

During the actual UVAG surface, it is difficult to count the number N_1. The number N in unit area (100 μm × 100 μm) on the surface is used to replace N_1. There are some differences between N_1 and N because of the overlapping of different grains. The degree of overlapping depends on grinding parameters (spindle speed n, feed rate V_s, cutting depth a_p and power ratio k). Therefore, an overlapping parameter k_4 ($k_4 = c_4 n^{a_{14}} V_s^{a_{24}} a_p^{a_{34}} k^{a_{44}}$) is introduced. The number N can be expressed as:

$$N = k_4 \cdot N_1 \tag{33}$$

3 Experiments and results

3.1 Experimental details

UVAG experiments are conducted on a machine which is DMG Ultrasonic 20 linear, DMG, Germany. The frequency of ultrasonic vibration is 23,540 Hz in this study. The amplitude of ultrasonic vibration is replaced by power ratio. When power ratio varies from 0 to 100%, vibration amplitude changes from about 0 to 5 μm. 100% of power ratio equals to 34 W. The outer diameter of diamond tool (provided by Schott Diamantwerkzeuge GmbH in Germany) is 8 mm, while wall thickness is 0.6 mm. And grain size is D126. Zirconia ceramics (provided by Qinhuangdao Aidite High-Technical Ceramics, Co., Ltd) is used as workpieces. The mechanical properties are shown in Table 2. Synergy 915 is used as an external coolant.

3.2 Obtaining k_0, k_1, k_2, k_3, k_4 and five surface feature parameters

Based on Eqs. (8), (12), (21), (22), (23), (24), (29), (30), (32) and (33), if the width d_w, depth h_d, length l_d, spacing d_f and number N of surface are measured through experiments, the parameters k_0, k_1, k_2, k_3 and k_4 can be obtained by the least square estimation (LSE) method. The experimental details for getting k_0, k_1, k_2, k_3 and k_4 are given in Table 3. The five parameters (d_w, h_d, l_d, d_f and N) are measured by laser microscope (KEYENCE, VK-X 100 series). In order to ensure the measurement accuracy of the width d_w, depth h_d, length l_d, spacing d_f and number N on the machined surface, every parameter measurement is repeated five times. The five parameters are measured in the center of specimen in the feed direction. The average value will be considered as the final value of d_w, h_d, l_d, d_f or N. When the number N is measured, the scale is 100 μm × 100 μm. UVAG surface topography is shown in Fig. 5. d_w, l_d, d_f and N are expressed in Fig. 5. h_d is the depth of one groove. k_0, k_1, k_2, k_3 and k_4 can be obtained as:

$$k_0 = 0.2802 n^{0.3203} V_s^{0.26347} \cdot a_p^{0.3601} \cdot k^{0.0830} \tag{34}$$

$$k_1 = 0.9167 n^{-0.1765} V_s^{-0.2403} a_p^{0.0594} k^{-0.9697} \tag{35}$$

$$k_2 = 480.7286 n^{-0.4739} V_s^{0.4675} a_p^{0.0711} k^{-0.0206} \tag{36}$$

$$k_3 = 0.0123 n^{1.2244} V_s^{0.6368} a_p^{0.0287} k^{0.4428} \tag{37}$$

$$k_4 = 4.8540 e^{-4} n^{1.0143} V_s^{-0.9483} a_p^{0.0030} k^{0.0461} \tag{38}$$

Table 3 Experimental details for getting k_0, k_1, k_2, k_3 and k_4

Group	Spindle speed n (r/min)	Feed rate V_s (mm/min)	Cutting depth a_p (mm)	Power ratio (%)
1	3000	50	0.015	50
2	4500	50	0.015	50
3	6000	50	0.015	50
4	4500	20	0.010	60
5	4500	30	0.010	60
6	4500	40	0.010	60
7	6000	40	0.010	80
8	6000	40	0.015	80
9	6000	40	0.020	80
10	5000	50	0.020	50
11	5000	50	0.020	70
12	5000	50	0.020	90

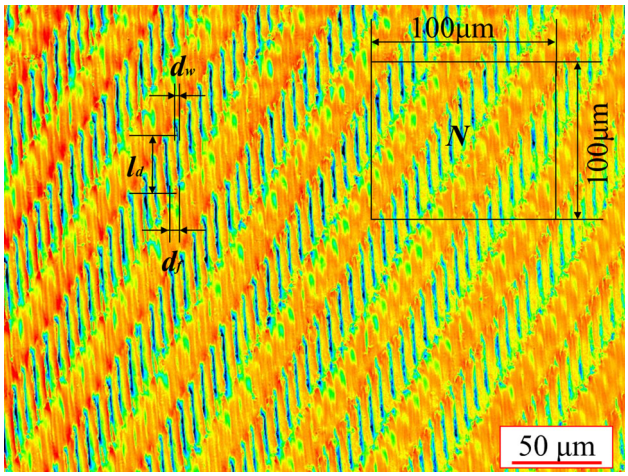

Fig. 5 UVAG surface topography in group five

Then, according to Eqs. (8), (12), (21), (22), (23), (24), (29), (30), (32), (33), (34), (35), (36), (37) and (38), five surface feature parameters (the width d_w, depth h_d, length l_d, spacing d_f and number N) can be derived as:

$$d_w = 0.0198n^{0.0604}V_s^{0.3420}a_p^{0.3601}k^{0.0830} \tag{39}$$

$$h_d = 0.0033n^{-0.3630}V_s^{-0.3024}a_p^{-0.1730}k^{-0.9697} \tag{40}$$

$$l_d = 0.002723n^{0.5261}V_s^{0.4675}a_p^{0.0711}k^{-0.0206} \cdot \left[\frac{\pi}{2} - \arcsin\left(1 - 1.1109n^{-0.2131}V_s^{0.0718}a_p^{-0.26565}\right)\right] \tag{41}$$

$$d_f = 0.0123n^{0.2244}V_s^{1.6368}a_p^{0.0287}k^{0.4428} \tag{42}$$

$$N = 4.8540e^{-4}n^{0.0143}V_s^{-0.9483}a_p^{0.0030}k^{0.0461}f \tag{43}$$

From Eqs. (39), (40), (41), (42) and (43), it can be seen that surface feature parameters are closely related to grinding parameters. d_w and d_f show positive exponential correlation with all the grinding parameters (spindle speed, feed rate, cutting depth and power ratio). The relationship between h_d and four grinding parameters is negative exponential. N, spindle speed, cutting depth and power ratio show positive exponential correlation, while it is negative exponential between N and feed rate. The relationship between l_d and grinding parameters is complicated. There is not only exponential relation but also arcsine relation between l_d and grinding parameters.

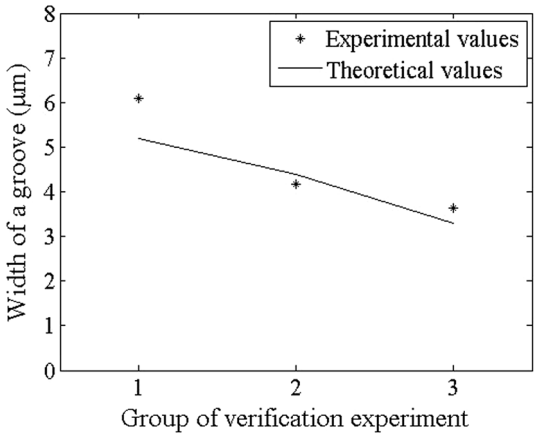

Fig. 6 Width verification

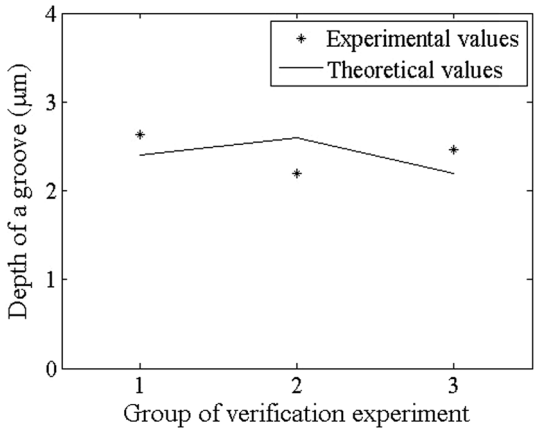

Fig. 7 Depth verification

3.3 Comparison between theoretical values and experimental values

The verification experiments are carried out, as shown in Table 4. The experimental values of width d_w, depth h_d, length l_d, spacing d_f and number N on the machined surface can be measured. According to Eqs. (39), (40), (41), (42) and (43), the theoretical values can be obtained. The comparison between theoretical values and experimental values is shown in Figs. 6, 7, 8, 9 and 10. It shows that the trends of theoretical values are consistent with those of experimental values.

Table 4 Verification experiments

Group	Spindle speed n (r/min)	Feed rate V_s (mm/min)	Cutting depth a_p (mm)	Power ratio (%)
1	7500	50	0.015	50
2	4500	50	0.010	60
3	6000	40	0.005	80

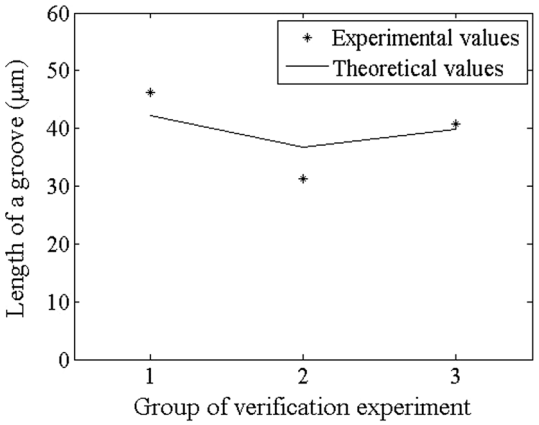

Fig. 8 Length verification

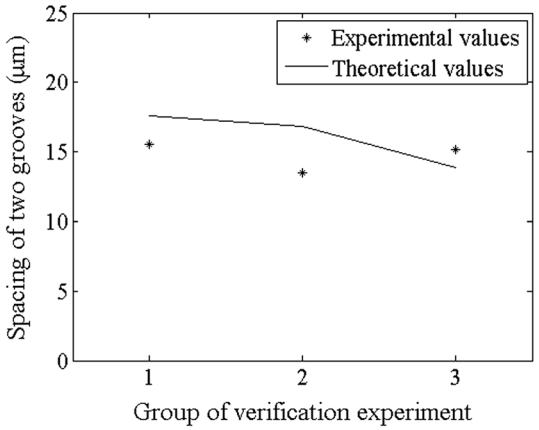

Fig. 9 Spacing verification

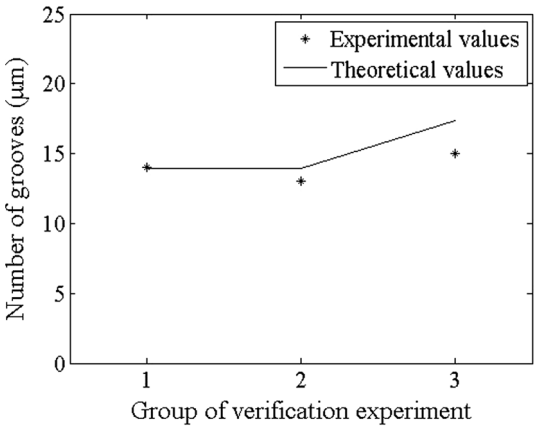

Fig. 10 Number verification

4 Conclusions

A mathematic modeling of five geometric parameters (width d_w, depth h_d, length l_d, spacing d_f and number N) for UVAG surface features of zirconia ceramics has been developed. The relationship between grinding parameters and five geometric parameters has been clarified theoretically. Finally, the experiments are conducted to verify the relationship. The conclusions are summarized as follows:

1. During the mathematic modeling, the overlapping of entire grains on the tool end face has been considered by calculating the expected value of center-to-center distance between two successive grooves and overlapping parameters. Grinding parameters have a close connection with the overlapping.
2. From the model, five geometric parameters (width d_w, depth h_d, length l_d, spacing d_f and number N) of UVAG surface have been obtained. It shows that d_w and d_f present exponential positive correlation with four grinding parameters, while h_d has a negative exponential correlation with grinding parameters. l_d has a complicated relationship with grinding parameters, and N is related to ultrasonic vibration frequency.
3. The theoretical values of mathematic modeling of five geometric parameters agree well with the experimental values. It provides a better understanding of characterizing surface topography of zirconia ceramics in UVAG.

In this work, it is innovative to put forward a mathematic model of geometric parameters for UVAG of zirconia ceramics. It can act as a reference for studying the surface topography of zirconia ceramics during UVAG.

Acknowledgements The authors appreciate the supports from the National Natural Science Foundation of China (Grant No. 51675284), China Scholarship Council (Grant No. 201706840056).

References

1. Gamborena I, Blatz MB (2006) A clinical guidelines to predictable esthetics with zirconium oxide ceramic restorations. Quintessence Dent Technol 29:11–23
2. Kosovka DD, Vesna M, Slobodan D, Dragan G (2013) Dilemmas in zirconia bonding: a review. Srp Arh Celok Lek 141(5–6):395–401
3. Preis V, Behr M, Handel G, Schneider-Feyrer S, Handel S, Rosentritt M (2012) Wear performance of dental ceramics after grinding and polishing treatments. J Mech Behav Biomed 10(6):13–22
4. Preis V, Grumser K, Schneider-Feyrer S, Behr M, Rosentritt M (2016) Cycle-dependent in vitro wear performance of dental ceramics after clinical surface treatments. J Mech Behav Biomed 53:49–58
5. Santos RLP, Buciumeanu M, Silva FS, Souza JCM, Nascimento RM, Motta FV, Carvalho O, Henriques B (2016) Tribological behaviour of glass-ceramics reinforced by yttria stabilized zirconia. Tribol Int 102:361–370
6. Liu YH, Wang Y, Wang DZ, Ma J, Liu LF, Shen ZJ (2016) Self-glazed zirconia reducing the wear to tooth enamel. J Eur Ceram Soc 36(12):2889–2894

7. Wang L, Liu YH, Si WJ, Feng HL, Tao YQ, Ma ZZ (2012) Friction and wear behaviors of dental ceramics against natural tooth enamel. J Eur Ceram Soc 32(11):2599–2606
8. Roy T, Choudhury D, Ghosh S, Mamat AB, Pingguan-Murphy B (2015) Improved friction and wear performance of micro dimpled ceramic-on-ceramic interface for hip joint arthroplasty. Ceram Int 41:681–690
9. Chirende B, Li JQ, Wen LG, Simalenga TE (2010) Effects of bionic non-smooth surface on reducing soil resistance to disc ploughing. Sci China Technol Sci 53(11):2960–2965
10. Kligerman Y, Etsion I, Shinkarenko A (2005) Improving tribological performance of piston rings by partial surface texturing. J Tribol 127:632–638
11. Li KM, Yao ZQ, Hu YX, Gu WB (2014) Friction and wear performance of laser peen textured surface under starved lubrication. Tribol Int 77:97–105
12. Tang W, Zhou YK, Zhu H, Yang HF (2013) The effect of surface texturing on reducing the friction and wear of steel under lubricated sliding contact. Appl Surf Sci 273:199–204
13. Segu DZ, Si GC, Choi JH, Kim SS (2013) The effect of multi-scale laser textured surface on lubrication regime. Appl Surf Sci 270(14):58–63
14. Wang QY, Liang ZQ, Wang XB, Jiao L (2016) Investigation on surface formation mechanism in elliptical ultrasonic assisted grinding (EUAG) of monocrystal sapphire based on fractal analysis method. Int J Adv Manuf Technol 87(9–12):2933–2942
15. Liang ZQ, Wang XB, Wu YB, Xie LJ, Jiao L, Zhao WX (2013) Experimental study on brittle–ductile transition in elliptical ultrasonic assisted grinding (EUAG) of monocrystal sapphire using single diamond abrasive grain. Int J Mach Tool Manuf 71(8):41–51
16. Wang Y, Lin B, Wang SL, Cao XY (2014) Study on the system matching of ultrasonic vibration assisted grinding for hard and brittle materials processing. Int J Mach Tool Manuf 77(1):66–73
17. Zhang JH, Wang LY, Tian FQ, Zhao Y, Wei Z (2016) Modeling study on surface roughness of ultrasonic-assisted micro end grinding of silica glass. Int J Adv Manuf Technol 86:407–418
18. Tesfay HD, Xu ZG, Li ZC (2016) Ultrasonic vibration assisted grinding of bio-ceramic materials: an experimental study on edge chippings with Hertzian indentation tests. Int J Adv Manuf Technol 86:3483–3494
19. Li ZH, Zheng K, Liao WH, Xiao XZ (2017) Tribological properties of surface topography in ultrasonic vibration-assisted grinding of zirconia ceramics. Proc Inst Mech Eng C J Mech 203–210:1989–1996
20. Yan YY, Zhao B, Liu JL (2009) Ultraprecision surface finishing of nano-ZrO2 ceramics using two-dimensional ultrasonic assisted grinding. Int J Adv Manuf Technol 43:462–467
21. Guo B, Zhao QL (2017) Ultrasonic vibration assisted grinding of hard and brittle linear micro-structured surfaces. Precis Eng 48:98–106
22. Marshall DB, Lawn BR, Evans AG (1982) Elastic/plastic indentation damage in ceramics: the lateral crack system. J Am Ceram Soc 65(11):561–566
23. Xiao XZ, Zheng K, Liao WH (2014) Theoretical model for cutting force in rotary ultrasonic milling of dental zirconia ceramics. Int J Adv Manuf Technol 75(9):1263–1277